Applications of Various Control Schemes on a Four-Bar Linkage Mechanism Driven by a Geared DC Motor

AHMAD AL-JARRAH, MOHAMMAD SALAH, SULEIMAN BANIHANI, KHALID AL-WIDYAN, and ANAS AHMAD
Department of Mechatronics Engineering
Hashemite University
JORDAN
msalah@hu.edu.jo

Abstract—Four-bar linkage mechanisms are of interest for many specialists in the academia and industry. However, it is one of the mechanisms that is highly nonlinear and exhibits complex behavior. Therefore, it is difficult to model and control their dynamic responses. In this paper, various control schemes are explored and tested on the four-bar mechanism to investigate the dynamical performance under different operating conditions. First, a filtered proportional-integral-derivative controller was implemented on the mechanism and then compared with a filtered sliding mode controller, filtered fuzzy controller, and filtered genetic-based reinforcement neurocontroller. An experimental setup was built and designed at the Hashemite University to explore practically different techniques to control the position and speed of the driving link in the four-bar linkage mechanism. The main challenge in controlling the mechanism is to overcome dynamic fluctuations due to system inertias. Preliminary simulation results showed that according to the operating conditions, some controller exhibit better performance over the others.

Keywords: control techniques; nonlinear systems; four-bar linkage; mechatronics.

1 Introduction

Four-bar mechanisms are used in a variety of industrial applications such as reciprocating compressor, rotary engine, scotch yoke, rope climbing robot, and robot end-effect gripper [1-3]. These mechanisms are usually applied to achieve a specific motion task such as path generation or rigid body guidance [1, 4, 5]. For example, in biomedical engineering, they are employed for accomplishing high-precision motion like micro-surgery application [6]. Many design difficulties could be created from such mechanisms; for example, the accuracy of the end-point positioning of a robot arm is considerably small because of the accumulated error from each revolute joint of the robot. In addition, having a poor mechanical stiffness will result in deterioration in the accuracy of the motion tracking [1].

The mathematical model and synthesis of these mechanisms are well known in many mechanics resources. However, one of the incorrect assumptions in the analysis and synthesis of such mechanisms is that the angular velocity of the crank is assumed to be constant. This may not be the case when the mechanism is driven by an electric motor through a gearbox. The angular speed on the crank of the four-bar mechanism shows a periodically changing behavior due to the changes in inertia effects during the rotation of rigid links forming the mechanism [4, 7].

As a result of such fluctuating behavior, the dynamics of a four-bar system is highly nonlinear, time-variant, and complex. This produces difficulties for control engineers in designing a control law to make the four-bar mechanism follows a desired trajectory precisely at high speeds. Several methods reported in literature proposed to handle those difficulties. For example, Lin and Chen [8] proposed a control structure for the four-bar that was composed of several sub-control algorithms such as a model reference adaptive control, a disturbance compensation loop and a modified switching controller, plus some feedback loops. In [6], an enhanced adaptive motion tracking control methodology without a feed-forward compensation was introduced for piezo-actuated flexure-based four-bar micro/nano manipulation mechanisms due to their nonlinear effect. Moreover, Erenturk [7] proposed a fuzzy logic controller combined with grey system modeling approach to reduce the angular speed fluctuations in four-bar mechanisms driven by a permanent magnet dc motor that is fed from a dc–dc converter.

Other researchers focused on the synthesis of mechanisms for tracking trajectories; which is a

well-known numerical optimization problem explored in depth in the literature. For instance, Yan [9] proposed an integrated mechanism and controller design approach to design variable input-speed servo four-bar linkages. The dimensions of the links, the counterweights, input speed trajectory, and controller parameters are considered as the design variables to reduce the shaking force and moment, to improve the speed trajectory tracking performance, and to minimize the motor power dissipation. Moreover, Sanchez-Marquez *et al.* [10] presented a modified harmony search (HS) algorithm for the synthesis of a four-bar planar mechanism that follows a specific trajectory where [11] employed genetic algorithms for optimum synthesis of a four-bar linkage and [12] described the process of optimal synthesis of a four-bar linkage by the method of variable controlled deviations with the application of the differential evolution algorithm.

On the other hand, other techniques were proposed to model four-bar mechanisms. In [13, 14], a parallelogram closed-loop mechanism was implemented into an open-loop robot structure to simplify the dynamics model of the overall system. High motion tracking performance was thus achieved by applying relatively simple control algorithms. Later, Diken [15] improved the motion tracking performance of the system by applying a mass redistribution scheme. In his study, the structure of a robot arm was first reduced to dynamically equivalent point masses to eliminate the gravitational term in the dynamic model. A simple algorithm was then applied to control the system, and satisfactory trajectory tracking can be obtained.

In this paper, various control schemes are tested and applied, in simulation, on a four-bar linkage mechanism to investigate performance and response improvement. First, a filtered proportional-integral-derivative controller (FPIDC) is tuned and implemented on the mechanism and then compared with a filtered sliding mode controller (FSMC), filtered fuzzy controller (FFC), and filtered genetic-based reinforcement neurocontroller (FGRNC). The proposed controllers never explored for such mechanism in the literature. Just few literature were found about only the fuzzy logic controller.

A four-bar linkage mechanism test bench was designed and assembled at the Hashemite University to conduct experimental testing as shown in Fig.1. However, the authors intend to explore and propose more control strategies in the future to more investigate the performance of such mechanism under various operating conditions. The test bench featured an aluminum rigid four-bar linkage, a geared dc motor (Maxon 24V, 1A, 4180rpm, and a 23:1 gear ratio), rotary incremental encoder (Autonics 5000 p/r), MOSFET-based High-Power Motor Driver (Pololu 24v23 CS), and a data acquisition card (NI9401 8-Channel TTL Digital Input/Output Module). All data acquisition and control operations were implemented using National Instruments board and interfaced with LabVIEW which allowed for real-time execution of the control/operation strategy. The LabVIEW coding permitted flexibility to implement various operation algorithms and permitted the capture of experimental results easily.

The flow of the paper is as follows: Section 2 introduces the mathematical modeling for a four-bar mechanism. Sections 3, 4, 5, and 6 present the FPIDC, FSMC, FFC, and FGRNC, respectively. Section 7 discusses the numerical simulation results. Finally, concluding remarks are presented in Section 8.

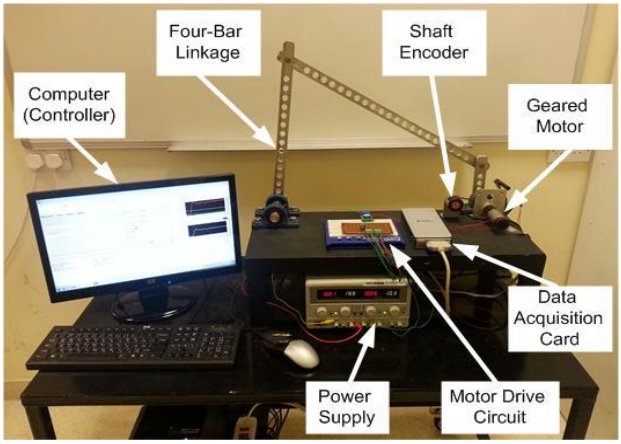

Fig.1: Experimental four-bar mechanism test bench

2 Four Bar Linkage Mathematical Model

A schematic of the four-bar linkage mechanism is shown in Fig.2. The proposed mechanism is driven by a geared permanent magnet dc motor. The mechanism is operated by controlling the dc motor voltage input that is connected to the first link of the mechanism, L_2. From Fig.2, the complete mathematical model of the mechanism can be developed. As reported in [7], the following mathematical expressions were developed to describe the motion of the mechanism and its behavior

$$\begin{aligned} T &= A\ddot{\phi}_2 + \frac{1}{2}\frac{dA}{d\phi_2}\dot{\phi}_2^2 + k\gamma_4\left(\phi_4 - \phi_4(0)\right) + C\gamma_4^2\dot{\phi}_2 \\ &= nT_m - nT_L - n^2B\dot{\phi}_2 - n^2J\ddot{\phi}_2 \end{aligned} \quad (1)$$

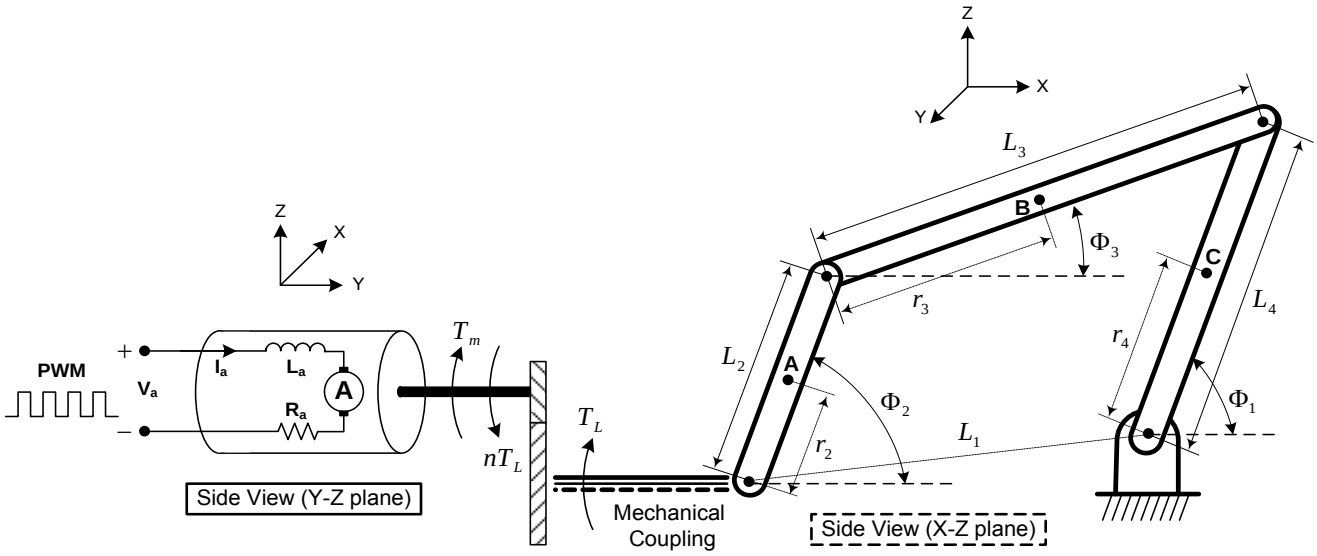

Fig.2. A schematic of the four-bar linkage mechanism driven by a geared permanent magnet dc motor

$$V_a = L_a \frac{di_a}{dt} + i_a R_a + n k_b \phi_2 \tag{2}$$

where $T_m = k_m i_a$.

Based on the torque equilibrium and the kinetic-potential equations with Lagrange's constraints, equation (1) was developed to represent the mechanical motion. All details of the mathematical model can be found in Appendix I.

Equation (2) was developed based on Kirchoff's voltage law for the geared permanent magnet dc motor. Note that *k* and *C* in equation (1) are attached to the follower to represent a general loading situation. The angular velocity of link *i* can be computed by $\dot{\phi}_i = \gamma_i \dot{\phi}_2 \ \forall \ i = 2,3,4$ where γ_i is defined in Appendix 1. The function A and its derivative with respect to angular position, $dA/d\phi_2$, are defined as well in Appendix 1. It should be noted from equations (1) and (2) that the entire mechanism is controlled by the applied armature voltage, which controls internally the armature current. The armature current certainly controls the induced torque of the motor that operates the mechanism.

The mathematical model of the four-bar linkage mechanism introduced in equations (1) and (2) with all definitions in Appendix 1 is complex and exhibits several highly nonlinear and time-variant terms. It is certain that the model equations depend on parameters that might be absent or difficult to be measured, such as, damping, spring, friction coefficients, and motor constants, therefore, it would be a challenging task to control such system.

3 Filtered Proportional-Integral-Derivative Control

In this section, a modified version of a standard PID is introduced to improve performance and reduce sensitivity to vibration phenomena in the four-bar linkage mechanism. As a matter of fact, the mechanical coupling of rigid bodies prevents an effective utilization of standard PID controller due to vibrations and inertias. The introduced filtered proportional-integral-derivative controller (FPIDC) is expressed as

$$u = \frac{\alpha}{\tau s + 1}\left\{k_p e + k_i \int e + k_d \dot{e}\right\} \tag{3}$$

where k_p, k_i, and k_d are the controller gains, α and τ are filter constants and are tuned to reduce fluctuations in controller output while regulating the actual system output.

4 Filtered Sliding Mode Control

A filtered sliding mode controller (FSMC) is proposed to control the four bar mechanism system. The proposed control objective is to ensure that the actual crank output (*i.e.*, speed, $\dot{\phi}_2$, or position, ϕ_2) tracks a desired input trajectory (*i.e.*, $\dot{\phi}_{2d}$ or ϕ_{2d}).

SMC is a special case of variable structure control and it is one of the robust controllers that are used in a wide range of areas such as robotics and aerospace. The advantage of using SMCs is that they are insensitive to system parameter uncertainties (*i.e.*,

modeling errors and disturbances) [16, 17]. However, SMCs exhibit a chattering phenomenon that may cause saturation and heats [16]. In order to reduce or eliminate the oscillations, boundary layer method is utilized as reported in the literature [16].

Fig.3 shows a phase portrait for the SMC action where two modes are recognized; the reaching mode and the sliding mode. The reaching mode is moving from point A until reaching the sliding surface (*i.e.*, entering the sliding mode). In the sliding mode, the controller is switching between two values based on the switching law until reaching zero error.

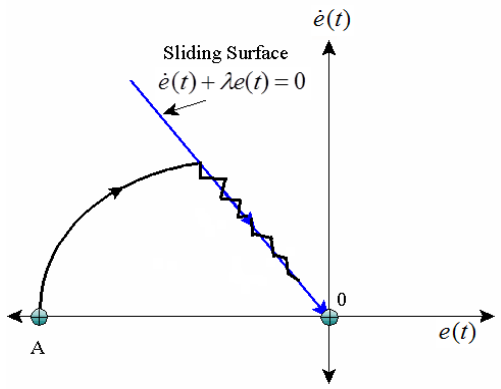

Fig.3: Phase plane portrait showing SMC action

The SMC can be recognized in the form of a relay control law as follows:

$$u=\begin{cases}V_1, & s>0\\ V_2, & s<0\end{cases} \tag{4}$$

where the parameters V_1 and V_2 are positive control gains, s is the linear sliding surface (*i.e.*, the switching function) and can expressed as

$$s=\lambda e+\dot{e} \tag{5}$$

where λ is a positive constant that represents the slope of the sliding surface, e and $\dot{e}$ are the error and its first time derivative. The error e is the difference between the desired and actual crank speed/position.

As mentioned earlier, in the sliding mode, the controller switches between two values. This switching causes a chattering phenomenon which causes in turn a high frequency of the control device. This indeed affects its functionality over a short period of time (*i.e.*, high controller activity cost). Hence, chattering is undesirable and should be eliminated or minimized for practical controller implementations. Other practical forms of SMC can be proposed instead in order to reduce the effect of chattering like SMC with boundary layer as shown in Fig.4. The action of SMC with parallel boundary layer is shown in Fig.4.a where the switching control law is given by

$$u=\begin{cases}V_1, & s>\alpha\\ V_2, & s<\alpha\end{cases} \tag{6}$$

The switching is made based on the value of α that is a positive constant and represents the parallel boundary layer. In Fig.4.b, another type of boundary layer is presented where two sliding surfaces s_1 and s_2 are used. The control action in this case is given by

$$u=\begin{cases}V_1, & s_1>0\\ V_2, & s_2<0\end{cases} \tag{7}$$

such that $s_1=\lambda_1 e+\dot{e}$ and $s_2=\lambda_2 e+\dot{e}$. It is clear that the switching function using the boundary layer techniques reduces the chattering since it delays the switching between the controller values.

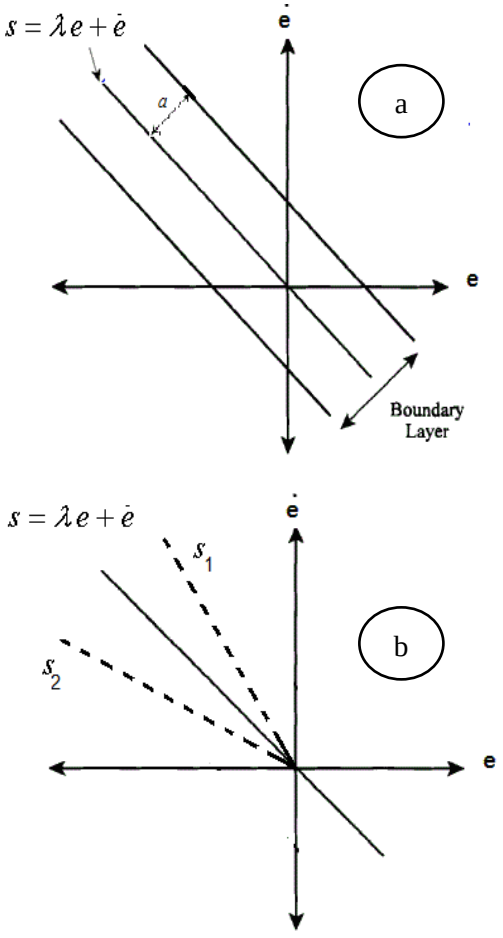

Fig.4: Types of boundary layers

However, a FSMC may perform better than any other types introduced earlier and can be represented as

$$u = \frac{\alpha}{\tau s + 1}\begin{Bmatrix} V_1, & s > 0 \\ V_2, & s < 0 \end{Bmatrix} \quad (8)$$

5 Filtered Fuzzy Control

In general, fuzzy control is a soft computing technique which imitates the ability of the human mind to learn and make rational decisions [7, 18]. It is a non-model-based control that features the simplicity of implementation and effectiveness in the cases of nonlinear and time-varying systems in comparison with other control methods.

In this section, a filtered fuzzy controller (FFC) is designed and introduced to effectively operate the four-bar linkage mechanism and regulate the driving link's position and speed. The filter is utilized to improve the output response of the four-bar linkage mechanism by smoothening the fluctuations of the control signal. Fig.5 shows a block diagram for the filtered fuzzy logic-based control system. The design of the proposed FFC is based on expert knowledge about the system to be controlled. Basically, it converts the linguistics information into control strategy.

The input variables to the fuzzy controller is the error signal, e, and its first time derivative, $\dot{e}$. The error signal is defined to be the difference between the desired input (*i.e.*, speed or position) and the actual output of the driving link of the mechanism (*i.e.*, speed or position). The input/output relationship is obtained from the fuzzy logic rules (*i.e.*, If-Then rules). The introduced fuzzy rules are designed and listed in Table 1 where NL: negative large, N: negative, Z: zero, P: positive, and PL: positive large. Note that the values inside the table indicate the nature of control signal (*i.e.*, motor input voltage). As an example from the table, if the error and its first time derivative are both NL, then the control output value should be NL.

Table 1. Proposed fuzzy rules

		$\dot{e}$				
		NL	**N**	**Z**	**P**	**PL**
e	**NL**	NL	NL	NL	N	P
	N	NL	N	N	Z	P
	Z	NL	N	Z	P	PL
	P	N	Z	P	P	PL
	PL	Z	P	PL	PL	PL

In the designed FFC, the triangle type is used for the membership functions for all variables in the fuzzification step due to its ease of implementation. The ranges of the membership functions are designed to be [-7, 7] for the error, [-130,130] for the first time derivative of error, and [-24, 24] for the output voltage. Finally, the fuzzy results obtained from the rules listed in Table 1 must be defuzzified to get the final control output crisp value. For this purpose, the center of area (COA) method proposed by Mamandi is used.

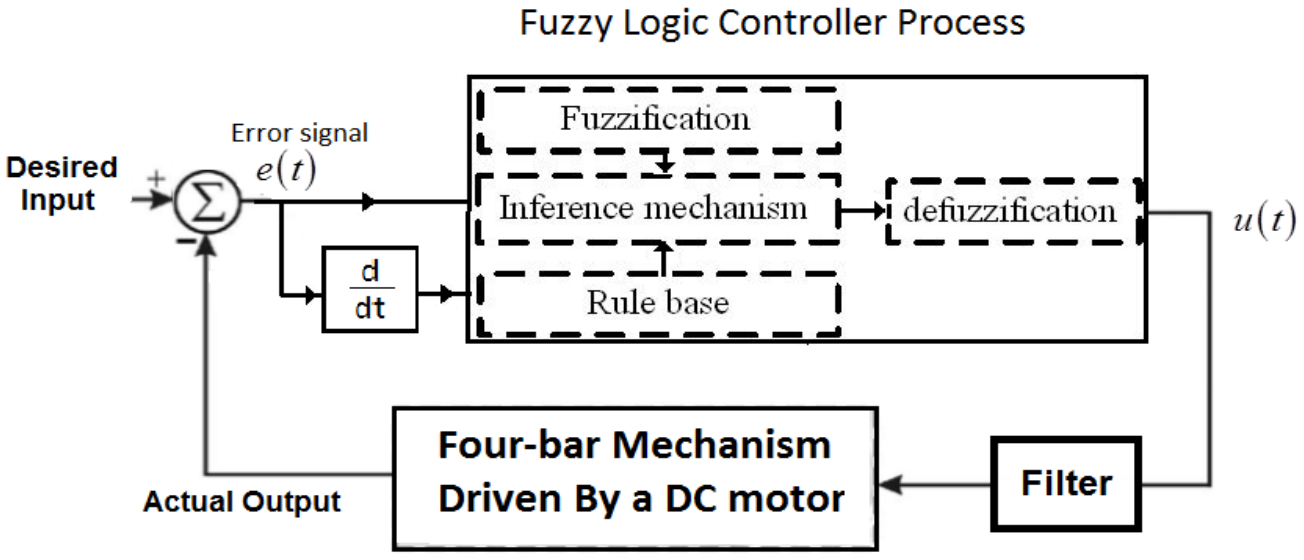

Fig.5. Block diagram of the fuzzy logic-based control system.

6 Filtered Genetic-Based Reinforcement Neurocontroller Design

In this section, a neurocontroller is proposed to regulate the speed of the driving link of the four-bar mechanism. The proposed neurocontroller is considered to be one of the artificial intelligence controllers classes where an artificial neural network (ANN) is utilized in the design. The ANN is trained to provide suitable control commands to achieve desired output performance.

There are three main types of neurocontrollers [19, 20]: (i) model-based control, (ii) Inverse model-based control, and (iii) reinforcement control. The first two types require the system model or inverse model to be known. Hence, data of system input/output has to be collected along with the internal states that may affect the output in addition to their time history (*i.e.*, previous states from last time steps). An ideal training set is almost impossible to acquire. In most cases it is desirable to train the neurocontroller on several training sets to reach acceptable performance. Another tedious task is to determine the architecture of the neural network itself (*i.e.*, number of hidden layers, neurons, neuron connections, and activation functions).

As for the reinforcement control, it does not require a prior knowledge of system model or its inverse. The controller is adapted according to its performance as it is the case in genetic algorithms (GAs). A GA is a natural inspired search and optimization technique in which, at each iteration, a population of candidate solutions (*i.e.*, potential neurocontrollers) competes according to their fitness (*i.e.*, performance) to be selected as "parents for the next generation". The process is terminated when the desired fitness or the maximum number of generations is reached. In other words, the main objective of the GA is to find the best NN structure (*e.g.*, in terms of number of hidden layers, hidden neurons, and weights) that produces the best performance while regulating the speed of the driving link of the four-bar linkage mechanism. Fig.6 shows a block diagram for the proposed GA-based reinforcement neurocontroller with tapped delay lines (TDL) (*i.e.*, history recording) for appropriate operation of the neurocontroller. Fig.7 illustrates the process of generating the best neurocontroller with the best performance.

As shown in Fig.7, the process of generating the best neurocontroller with the best performance starts with randomly generating a population of "n" reinforcement neurocontrollers with different structure (*i.e.*, hidden layers and neurons). Next, the fitness (*i.e.*, performance) of each individual neurocontroller is measured according to its ability to control the process in hand (*i.e.*, regulate the speed of the driving link of the four-bar linkage mechanism). The individual tested neurocontroller are then arranged according to the obtained fitness to be selected as "parents" for the next generation of improved neurocontrollers. Parents are selected to generate new neurocontrollers (*i.e.*, offsprings) according to their fitness in a process called rank selection, where members of higher fitness have more chance to be chosen as parents for the next generation. Offsprings are produced from parents. The chromosome (*i.e.*, population genetic material) of the parents", where all the information about the controller is encoded, are modified using genetic operators (*i.e.*, crossover and mutation). Offspring replaces their parents to create a new population. Again, the fitness of the new members is calculated, if the desired fitness is achieved, then the process is terminated and the member of the highest fitness is the suitable neurocontroller for the system. Otherwise, step 3 will be implemented again and the process is repeated until the maximum number of generations is reached.

The input variable to the neurocontroller is only the error signal (*i.e.*, the difference between the desired speed/position and actual speed/position). The output of the neurocontroller is the desired motor voltage required to minimize the error and achieving the desired motor speed.

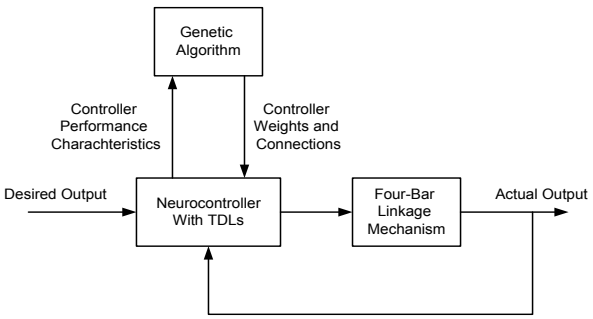

Fig.6: A block diagram for the genetic-based reinforcement neurocontroller

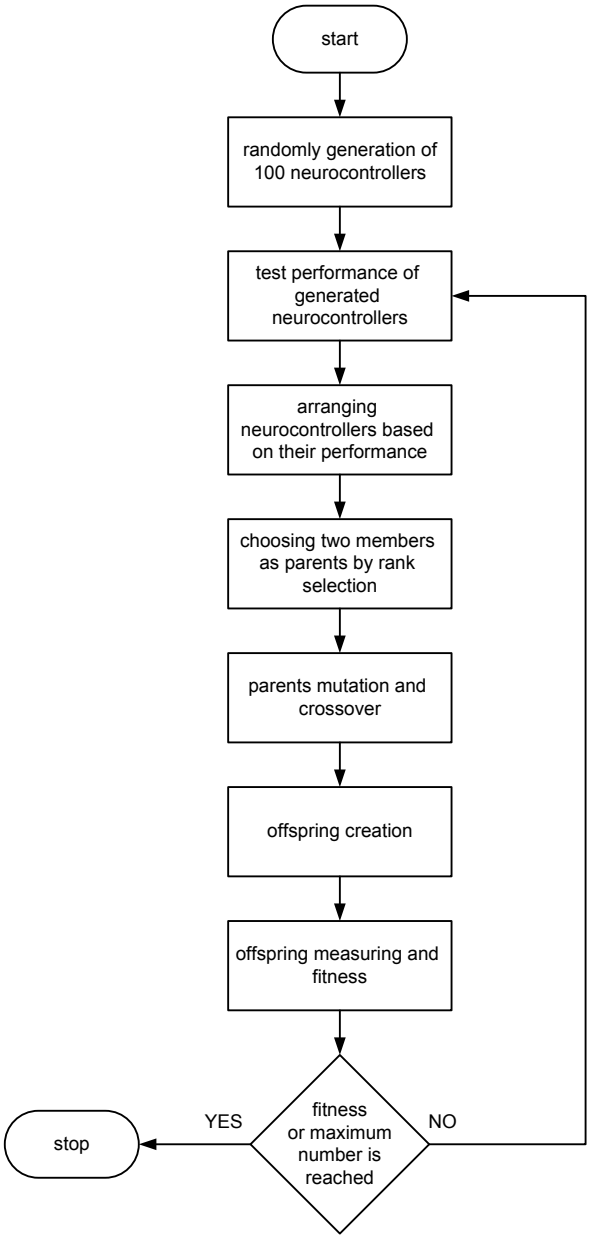

Fig.7: Flow chart of the process of generating a genetic-based reinforcement neurocontroller.

7 Simulation Results

Simulation results are presented in this section to evaluate the performance of the proposed control techniques. Fig.8 shows an open-loop step response of the crank angular velocity when applying an input voltage of 5V to the mechanism driving motor. It is obvious that the speed fluctuates between 6 to 9.6 rad/sec; and that is because of the continuous fluctuating of the system inertia at different angles of the crank joint. Hence, FPIDC, FSMC, FFC, and FGRNC schemes are used to improve the speed response of the mechanism and reduce fluctuations. For all subsequent simulated tests, a band limited white noise of power 1μ is applied on the feedback signals to have realistic measurements. Moreover, a saturation function with limits of ±24V (*i.e.*, motor rated voltage) has been applied at the output of controllers to add more reality to the physical system. The simulation was implemented with Bogacki-Shmpine (ode3) solver and 300μ sec sampling time. Table 2 shows all parameter values of the four-bar linkage mechanism.

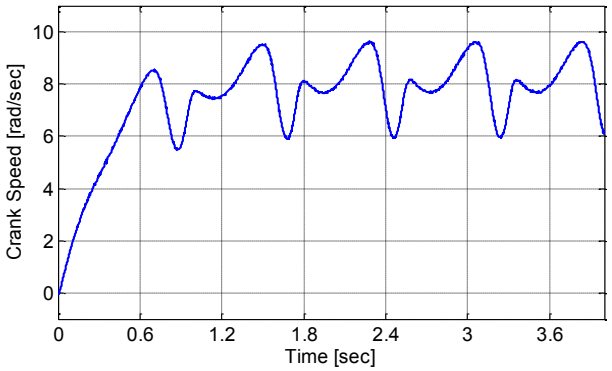

Fig.8: Crank speed for open-loop system when 5V input voltage is applied.

Table 2: Simulation parameter values for the introduced four-bar linkage mechanism

Parameter	Value	Parameter	Value
B	0	m_2	0.09919
C	0	m_3	0.1794
J	0.011	m_4	0.1765
J_2	0.000269	n	0.95
J_3	0.00219	$\phi_2(0)$	1.5708
J_4	0.00229	$\phi_3(0)$	0.5196
k	0	$\phi_4(0)$	$\frac{\pi}{2}$
k_b	0.26	r_2	0.0674
k_m	0.26	r_3	0.1488
L_2	0.1349	r_4	0.1625
L_3	0.2997	R_a	2
L_4	0.3251	T_L	0.28
L_a	0.014		

Four cases for speed and position control have been investigated and implemented in simulation to explore the performance of the introduced controllers as listed in Table 3. As shown from Table 3, cases I and II (*i.e.*, speed control) are

introduced to investigate the response of mechanism at relatively low and high speeds. In cases III and IV (*i.e.*, position control), the comparison is between a desired fixed link position with a swinging link (*i.e.*, driving link of the mechanism to track a trajectory). Four controllers have been implemented to explore their effectiveness in regulating the speed and position of the four-bar linkage mechanism. Table 4 shows the settings of controllers used.

Table 3: Simulated cases of operation and control

Case	Control Type	Desired Tracking Profile
I	Speed Control	ω_d = 10 rad/sec (*i.e.*, 1.6 RPS)
II		ω_d = 7 rad/sec (*i.e.*, 1.1 RPS)
III	Position Control	$\theta_d = 2\pi$ rad
IV		$\theta_d = \frac{\pi}{6}\sin(3t)+\frac{\pi}{2}$ rad

Table 4: Setting of introduced controllers

Controller		Filter	Tuned Gains
FPIDC	Case II	$\frac{8}{0.2s+1}$	$k_p = 70,\ k_i = 0.1,\ k_d = 2$
	Case III	$\frac{0.2}{0.01s+1}$	$k_p = 60,\ k_i = 15,\ k_d = 6$
	Case IV		$k_p = 130,\ k_i = 15,\ k_d = 6$
FSMC	Case II	$\frac{8}{0.2s+1}$	$V_1 = 20,\ V_2 = -20,\ \lambda = 30$
	Case III	$\frac{0.3}{0.01s+1}$	
	Case IV		
FFC	Case II	$\frac{2}{0.01s+1}$	As shown in Table 1
	Case III		
	Case IV		
FGRNC	Case II	$\frac{8}{0.2s+1}$	As shown in Fig.6
	Case III	$\frac{2}{0.01s+1}$	
	Case IV		

Figs 9 to 12 show the speed response with motor input voltage using the FPIDC for both cases I and II, respectively. It is clear that at relatively high speed (*i.e.*, Case I) the motor has to reverse direction of rotation to overcome strong fluctuations due to inertia; and despite of that, 17% overshoot can not be avoided and absolute tracking error of 0.1 rad/sec is observed. On the other hand, at relatively low speeds (*i.e.*, Case II), crank speed response is smooth and no overshoot is observed with an absolute tracking error of 0.06 rad/sec. Moreover, motor rotates in the same direction and still can overcome fluctuations due to inertia. In both cases I and II, the controller changes the voltage polarity at the beginning of operation but with bigger values for case I.

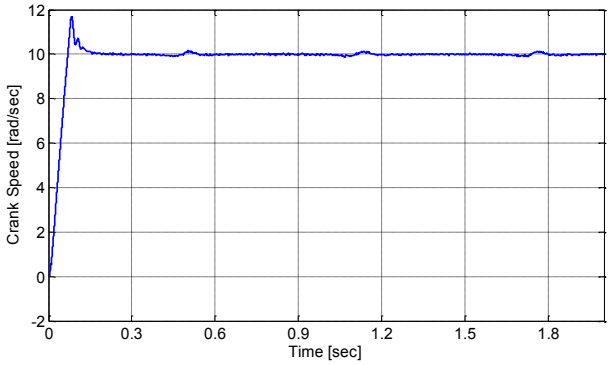

Fig.9: Crank speed using FPIDC for Case I

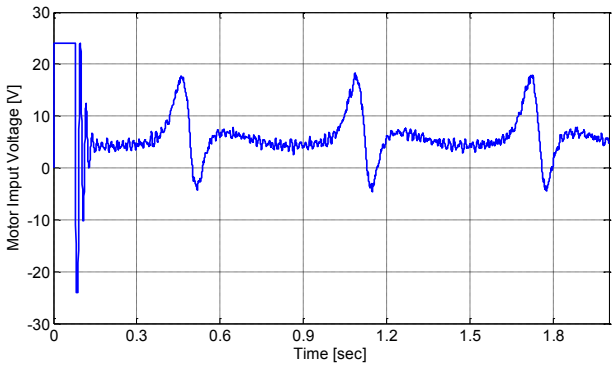

Fig.10: Motor input voltage using FPIDC for Case I

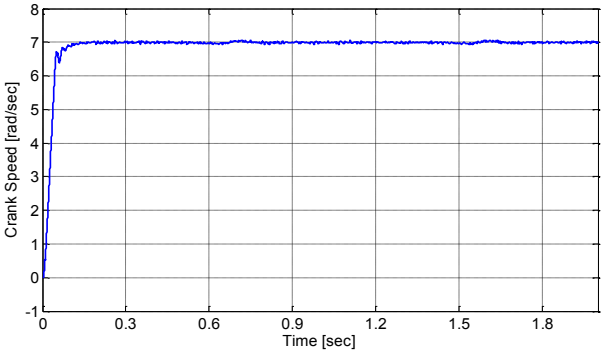

Fig.11: Crank speed using FPIDC for Case II

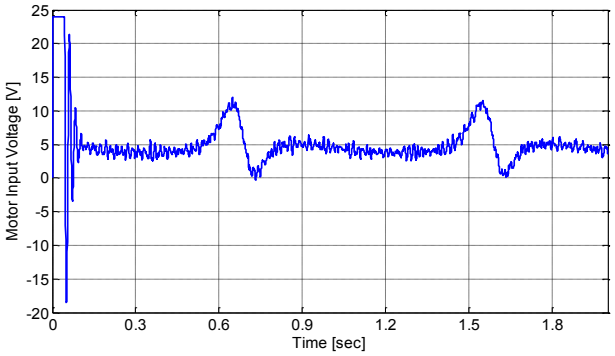

Fig.12: Motor input voltage using FPIDC for Case II

Figs 13 and 14 introduce the responses of mechanism crank speed and motor input voltage using FSMC for Case II, respectively. It is very clear how smooth the speed response is with absolute tracking error of 0.04 rad/sec. The motor input voltage does not reverse polarity at any time of operation. However, the fluctuations in motor input voltage are more in comparison with the FPIDC.

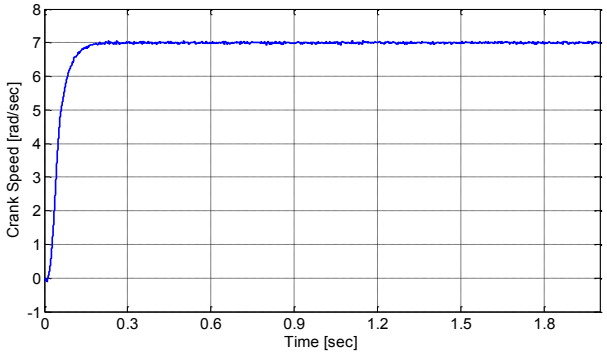

Fig.13: Crank speed using FSMC for Case II

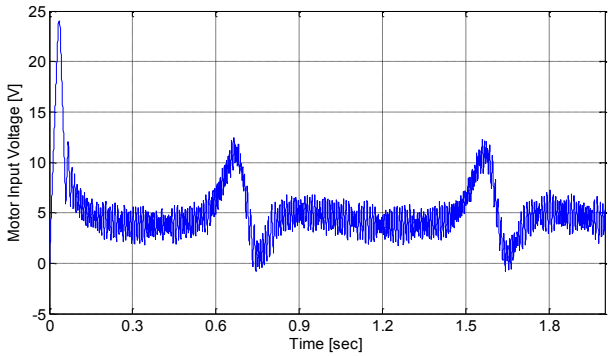

Fig.14: Motor input voltage using FSMC for Case II

Moreover, Figs 15 to 18 introduce the responses of mechanism crank speed and motor input voltage using FFC and FGRNC for Case II, respectively. It is very clear the smooth but slow response of speed using the FFC. However, even more fluctuations in the motor input voltage, in comparison with other controllers, occur with an absolute tracking error of 0.1 rad. On the other hand, FGRNC performs the best in terms of motor input voltage fluctuations while regulating the speed at 7 rad/sec in comparison with all other introduced controllers.

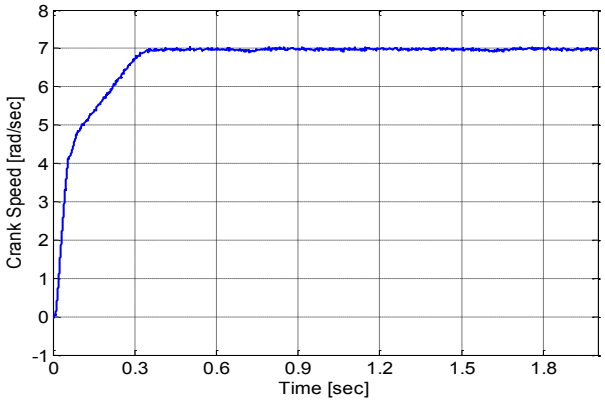

Fig.15: Crank speed using FFC for Case II

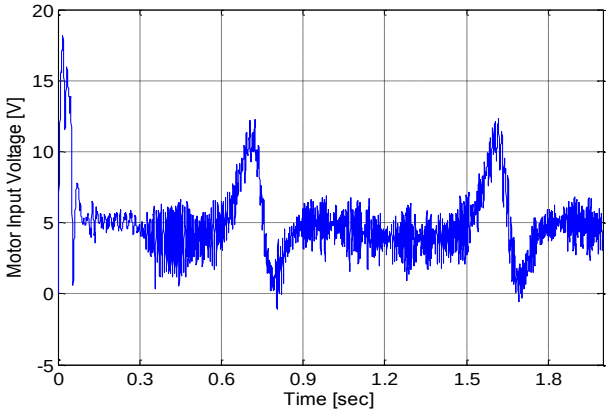

Fig.16: Motor input voltage using FFC for Case II

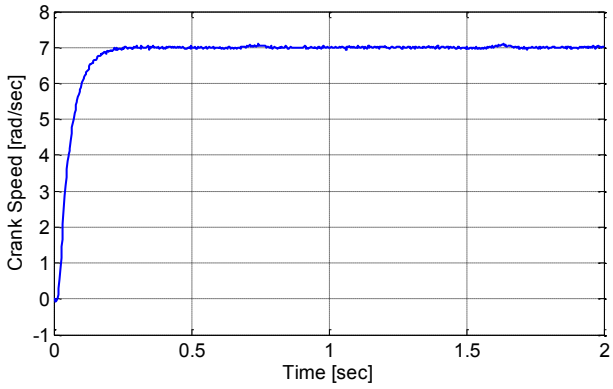

Fig.17: Crank speed using FGRNC for Case II

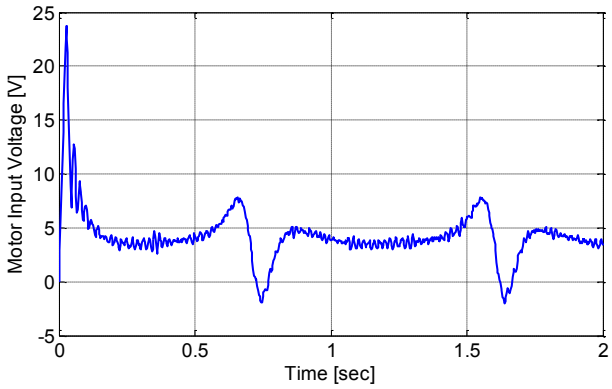

Fig.18: Motor input voltage using FGRNC for Case II

As for position control, Figs 19 to 26 show the crank position response and motor input voltage, respectively, for all controllers for Case III. It is very clear that FPIDC performs better than other controllers. FFC exhibits satisfactory response despite of the high overshoot in comparison with the FSMC and FGRNC. In general, FSMC performs the worst in terms of speed response time and fluctuations of the motor input voltage despite of its low absolute tracking error.

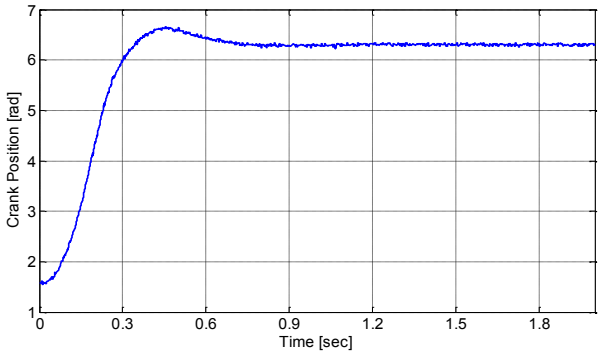

Fig.19: Crank position using FPIDC for Case III

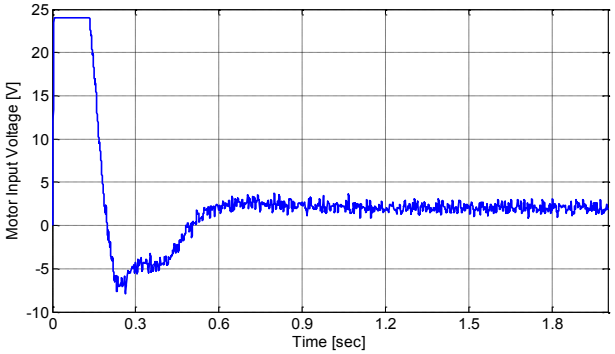

Fig.20: Motor input voltage using FPIDC for Case III

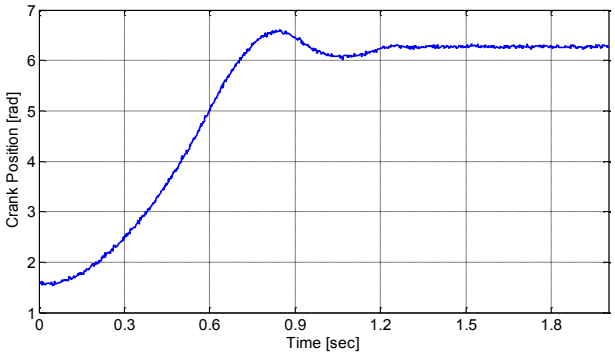

Fig.21: Crank position using FSMC for Case III

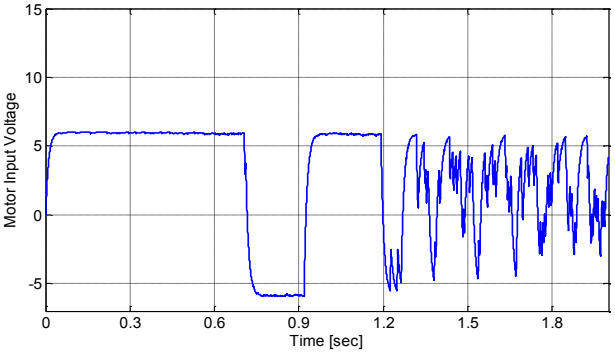

Fig.22: Motor input voltage using FSMC for Case III

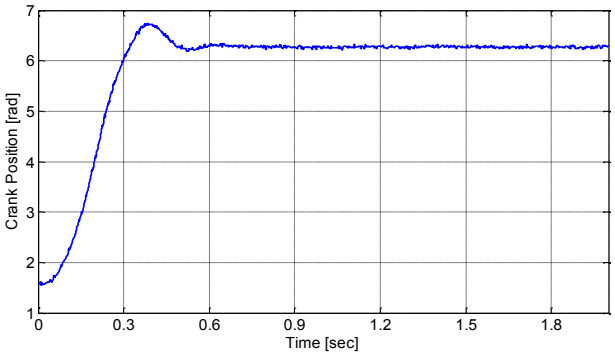

Fig.23: Crank position using FFC for Case III

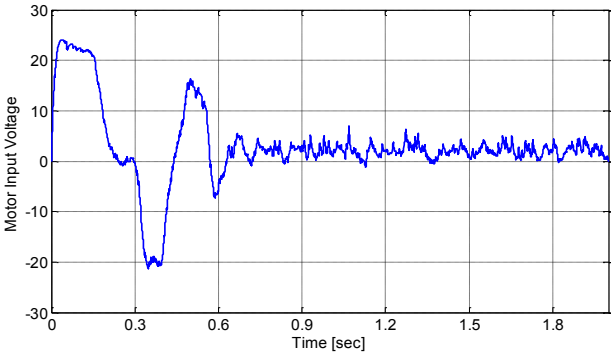

Fig.24: Motor input voltage using FFC for Case III

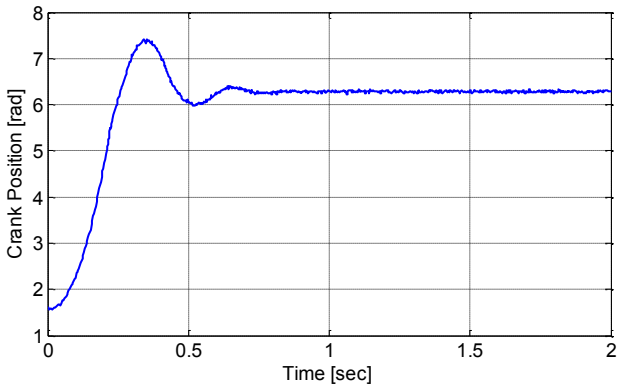

Fig.25: Crank position using FGRNC for Case III

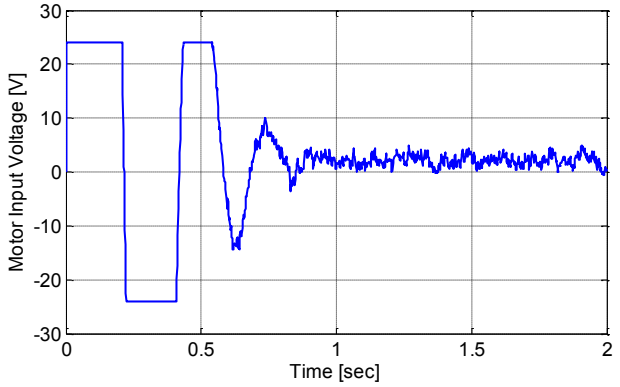

Fig.26: Motor input voltage using FGRNC for Case III

For Case IV, the motor input voltage responses for all controllers are presented through Figs 27 to 30. In this case, it is required to track a desired trajectory where the link is swinging back and forth in the same manner as a sinusoidal function. Since all responses look alike, Figs are not presented. As shown from Figs 27 to 30, FGRNC exhibits relatively the best performance in comparison with other controllers. The motor input voltage of the FGRNC almost does not change polarity and less fluctuating as well.

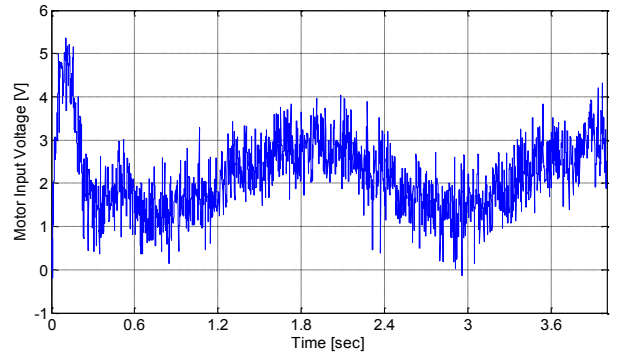

Fig.27: Motor input voltage using FPIDC for Case IV

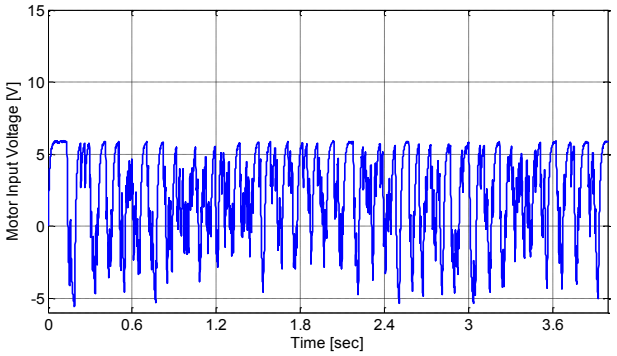

Fig.28: Motor input voltage using FSMC for Case IV

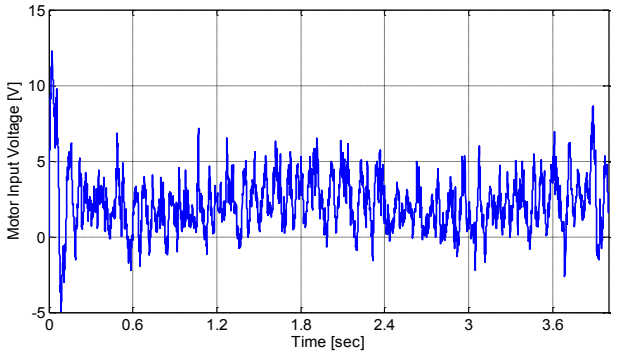

Fig.29: Motor input voltage using FFC for Case IV

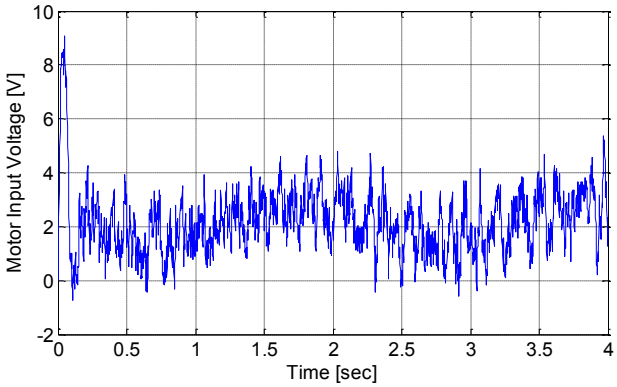

Fig.30: Motor input voltage using FGRNC for Case IV

Table 5 shows a quantitative comparison between the introduced controllers. The following two measures are computed to quantify the performance of each controller:

$$M_u = \int_0^T \left| u(\tau) \right|^2 d\tau \tag{9}$$

$$M_e = \int_0^T \left| e(\tau) \right|^2 d\tau \tag{10}$$

where M_u is the measure of energy expanded by the controller over the period of system operation (*i.e.*,

T = 2 for cases I, II, and III, T = 4 for Case IV). The variable M_e is the measure for tracking error over the same period of operation. From Table 5, it is clear how similar the controllers are in terms of absolute tracking error. The highest values were recorded for Case IV using FPIDC and Case II using FFC. Nevertheless, they are acceptable error values for the selected tracked setpoint(s). In general, the numbers listed in Table 5 are listed to provide in-depth quantitive measure for all cases using all controllers. Low measures do not mean that the controller is better. Its output voltage (*i.e.*, motor input voltage) may have relatively high fluctuations. It should be noted that good controller should exhibit low measures, less absolute tracking error, smooth voltage response, no overshoot or small one, and fast response or short transient response.

Table 5: Maximum absolute tracking error with controller effort and tracking error measures for different controllers

Controller		$\max\|e\|$	M_e	M_u
FPIDC	Case II	0.06	1.01	79.77
	Case III	0.05	3.17	99.70
	Case IV	0.13	0.022	22.08
FSMC	Case II	0.04	1.87	67.76
	Case III	0.045	8.23	49.22
	Case IV	0.06	0.0028	55.38
FFC	Case II	0.1	2.24	62.75
	Case III	0.045	3.36	139.3
	Case IV	0.05	0.0018	32.56
FGRNC	Case II	0.09	1.91	45.74
	Case III	0.045	3.10	240
	Case IV	0.06	0.0036	4.53

8 Conclusions

Different control techniques have been implemented in simulation to explore their effectiveness in regulating the speed and position of the four-bar linkage mechanism under different operating conditions. Despite of the challenges encountered due to the high nonlinearity and complexity of the mechanism dynamics, the introduced controllers are able to satisfactorily regulate the speed and position of the mechanism. Four controllers are proposed for this purpose and they all exhibit relatively adequate performance although some of them performs better than the other under some operating conditions.

Nomenclature List

A	=	A nonlinear function that represents inertia term
B	=	Vicious damping at motor bearing
C	=	Torsional damping coefficient
i_a	=	Motor armature current
J	=	Moment of inertia of the motor rotor and gear
J_i	=	Moment of inertia of the i^{th} link
k	=	Torsional spring constant
k_b	=	Motor electromotive force voltage constant
k_m	=	Motor torque constant
L_a	=	Motor armature inductance
L_i	=	Length of the i^{th} link
m_i	=	Mass of the i^{th} link
n	=	Gear ratio
ϕ_i	=	Angular position of the i^{th} link
$\dot{\phi}_i$	=	Angular velocity of the i^{th} link
$\ddot{\phi}_2$	=	Angular acceleration of the 2nd link
r_i	=	Location of center of the mass of the i^{th} link
R_a	=	Motor armature resistance
T	=	Total applied torque on link 2
T_L	=	Constant mechanical load
T_m	=	Motor output torque
V_a	=	Applied armature voltage (i.e., motor input voltage / controller output)

Appendix 1: Definitions

The function A and its derivative were developed in [2] to be

$$A = C_0 + C_1\gamma_3^2 + C_2\gamma_4^2 + C_3\gamma_3\cos(\phi_3 - \phi_2) \qquad (11)$$

$$\frac{dA}{d\phi_2} = 2C_1\gamma_3\frac{d\gamma_3}{d\phi_2} + 2C_2\gamma_4\frac{d\gamma_4}{d\phi_2} + C_3\ldots \left\{\frac{d\gamma_3}{d\phi_2}\cos(\phi_3 - \phi_2) - \gamma_3\sin(\phi_3 - \phi_2)(\gamma_3 - 1)\right\} \qquad (12)$$

where

$$\begin{aligned} C_0 &= J_2 + m_2 r_2^2 + m_3 L_2^2 \\ C_1 &= J_3 + m_3 r_3^2 \\ C_2 &= J_4 + m_4 r_4^2 \\ C_3 &= 2 m_3 r_3 L_2 \end{aligned} \tag{13}$$

and

$$\begin{aligned} \frac{d\gamma_3}{d\phi_2} &= \frac{L_2 (D_1 + D_2)}{L_3 \sin^2(\phi_3 - \phi_4)} \\ \frac{d\gamma_4}{d\phi_2} &= \frac{L_2 (D_3 + D_4)}{L_4 \sin^2(\phi_3 - \phi_4)} \end{aligned} \tag{14}$$

where

$$\begin{aligned} D_1 &= (\gamma_4 - 1)\sin(\phi_3 - \phi_4)\cos(\phi_4 - \phi_2) \\ D_2 &= (\gamma_4 - \gamma_3)\sin(\phi_4 - \phi_2)\cos(\phi_3 - \phi_4) \\ D_3 &= (\gamma_3 - 1)\sin(\phi_3 - \phi_4)\cos(\phi_3 - \phi_2) \\ D_4 &= (\gamma_4 - \gamma_3)\sin(\phi_3 - \phi_2)\cos(\phi_3 - \phi_4) \end{aligned} \tag{15}$$

and

$$\begin{aligned} \gamma_2 &= 1 \\ \gamma_3 &= \frac{L_2 \sin(\overline{\phi_4} - \phi_2)}{L_3 \sin(\phi_3 - \overline{\phi_4})} \\ \gamma_4 &= \frac{L_2 \sin(\phi_3 - \phi_2)}{L_4 \sin(\overline{\phi_4} - \phi_3)} \end{aligned} \tag{16}$$

and

$$\overline{\phi_4} = \phi_4 + \pi \tag{17}$$

References

[1] W. J. Zhang and X. B. Chen, Mechatronics design for a programmable closed-loop mechanism, *Proceedings of the Institution of Mechanical Engineers, Part C: Journal of Mechanical Engineering Science*, Vol.205, No.3, 2001, pp. 365–375.

[2] G. Rajesh Kanna and Ashik M., Design and development of a rope climbing robot using four bar mechanism with wireless control using TX2/RX2 RF module, *IEEE International Conference on Sign*al *Processing, Informatics, Communication and Energy Systems (SPICES)*, Feb. 2015.

[3] A. Hassan and M. Abomoharam, Design of a single DOF gripper based on four-bar and slider-crank mechanism for educational purposes, *24th CIRP design conference, Procedia CIRP*, Vol.21, 2014, pp. 379 – 384.

[4] O. Gundogdu and K. Erenturk, Fuzzy control of a dc motor driven four-bar mechanism, *Mechatronics*, Vol.15, No.4, 2005, pp. 423-438.

[5] S. Ebrahimi and P. Payvandy, Efficient constrained synthesis of path generating four-bar mechanisms based on the heuristic optimization algorithms, *Mechanisms and Machine Theory*, Vol.85, 2015, pp. 189-204.

[6] H. C. Liaw and B. Shirinzadeh, Enhanced adaptive motion tracking control of piezo-actuated flexure-based four-bar mechanisms for micro/nano manipulation, *Sensors and Actuators A: Physical*, Vol.147, 2008, pp.254-262

[7] K. Erenturk, Hybrid control of a mechatronic system: fuzzy logic and grey system modeling approach, *IEEE/ASME Transactions on Mechatronics*, Vol.12, No.6, 2007, pp. 703-710.

[8] M. Lin and J. Chen, Experiments toward MRAC design for linkage system, *Mechatronics*, Vol.6, No.8, 1996, pp. 933-953.

[9] Hong-Sen Yan, Guo-Jhih Yan, Integrated control and mechanism design for the variable input-speed servo four-bar linkages, *Mehcatronics*, Vol.19, 2009, pp. 274-285.

[10] A. Sanchez-Marquez, E. Vega-Alvarado, E. Alfredo Portilla-Flores, E. Mezura-Montes, Synthesis of a planar four-bar mechanism for position control using the harmony search algorithm, *11th International Conference on Electrical, Computing science and Automatic Control (CCE*), 2014.

[11] N. Nariman-Zadeh, M. Felezi, A. Jamali, and M. Ganji, Pareto optimal synthesis of four-bar mechanisms for path generation, *Mechanisms and Machine Theory*, Vol.44, No.1, 2009, pp. 180-191.

[12] R. Bulatovic and S. Dordevic, On the optimum synthesis of a four-bar linkage using differential evolution and method of variable controlled deviations, *Mechanisms and Machine Theory*, Vol.44, No.1, 2009, pp. 235-246.

[13] K. Youcef-Toumi, *Analysis, design and control of direct drive manipulators*, PhD dissertation, Mechanical Engineering

Department, Massachusetts Institute of Technology, 1985.

[14] K. Youcef-Toumi and A. Kuo, High-speed trajectory control of a direct-drive manipulator, *IEEE Transactions on Robotics and Automation*, Vol.9, No.1, 1993, pp. 102-108.

[15] H. Diken, Trajectory control of mass balanced manipulator, *Mechanisms and Machine Theory*, Vol.32, No.3, 1997, pp. 313-322

[16] Y.-F., Li, *High precision motion control based on a discrete-time sliding mode approach*, Ph.D. Dissertation, Department of Machine Design Royal Institute of Technology, Stockholm, Sweden, 2001.

[17] S. Nlwa, M. Kajitani, K. Sagimori, and K. Nakajima, Development of coordinated algorithm of EGR and boost pressure based on the adaptive sliding mode control, *SAE paper No. 2008-01-0996*, 2008.

[18] A. Al-Jarrah, M. Salah, and A. Al-Tamimi, Fuzzy logic control design for advanced vehicle thermal management system, *13th IASTED International Conference on Control and Applications*, Vancouver, BC, Canada, 2011, pp. 200-204.

[19] P. Spronck, Elegance, *Genetic Algorithms in Neural Reinforcement Control*, Master's Thesis, Delft University of Technology, The Netherlands 1996.

[20] D. Whitley, S. Dominic, R. Das, and C. W. Anderson, Genetic reinforcement learning for neurocontrol problems, *Machine Learning*, 13, 1993, pp. 259-284.